

Heterodyne broadband detection of axion dark matter

Asher Berlin¹, Raffaele Tito D’Agnolo², Sebastian A. R. Ellis³, and Kevin Zhou³

¹*Center for Cosmology and Particle Physics, Department of Physics, New York University, New York, New York 10003, USA*

²*Institut de Physique Théorique, Université Paris Saclay, CEA, F-91191 Gif-sur-Yvette, France*

³*SLAC National Accelerator Laboratory, 2575 Sand Hill Road, Menlo Park, California 94025, USA*



(Received 18 August 2020; accepted 1 December 2021; published 17 December 2021)

We propose a new broadband search strategy for ultralight axion dark matter that interacts with electromagnetism. An oscillating axion field induces transitions between two quasidegenerate resonant modes of a superconducting cavity. In two broadband runs optimized for high and low masses, this setup can probe unexplored parameter space for axionlike particles covering 15 orders of magnitude in mass, including astrophysically long-ranged fuzzy dark matter.

DOI: [10.1103/PhysRevD.104.L111701](https://doi.org/10.1103/PhysRevD.104.L111701)

I. INTRODUCTION

Evidence for dark matter (DM) has been accumulating for almost 90 years [1] and its microscopic nature remains one of the most important open questions in physics. Among the many DM candidates proposed in the literature, light pseudoscalar bosons with sub-eV masses have garnered considerable appeal since they generically appear in string compactifications [2–4] and have a simple and predictive cosmological history. Furthermore, in certain regions of parameter space they can solve the strong CP [5–11] or electroweak hierarchy problem [12–14]. In the “fuzzy” mass limit ($m_{\text{DM}} \sim 10^{-22}$ eV), light bosonic DM may also play a role in resolving long-standing tensions between observations and simulations of galactic structure [15–17]. In this work, we present a new detection strategy for these DM candidates, which we refer to as axions.

Axion DM generically couples to electromagnetism through the interaction

$$-\mathcal{L} \supset \frac{1}{4} g_{a\gamma\gamma} a F_{\mu\nu} \tilde{F}^{\mu\nu} \supset \frac{1}{2} \mathbf{J}_{\text{eff}} \cdot \mathbf{A}, \quad (1)$$

where a is the axion field and \mathbf{A} is the vector potential. In the presence of a background magnetic field \mathbf{B} , the axion sources an effective current density

$$\mathbf{J}_{\text{eff}} \simeq g_{a\gamma\gamma} \partial_t a \mathbf{B}. \quad (2)$$

Published by the American Physical Society under the terms of the Creative Commons Attribution 4.0 International license. Further distribution of this work must maintain attribution to the author(s) and the published article’s title, journal citation, and DOI. Funded by SCOAP³.

The interaction of Eq. (1) forms the basis of several experimental approaches to axion detection [18–33]. For instance, the time variation of \mathbf{J}_{eff} may be used to drive a resonant detector [34,35]. Such experiments exploit the coherence properties of the axion DM field, which we model as a classical Gaussian random field within the galaxy, with an average local density $\rho_{\text{DM}} \simeq 0.4$ GeV/cm³ and oscillating with angular frequency approximately equal to the axion mass m_a . Velocity dispersion from virialization within the galaxy leads to a spectral broadening of the axion, with a characteristic width of $\Delta\omega_a \sim m_a/Q_a$, where $Q_a \sim 10^6$.

In setups applying static magnetic fields, \mathbf{J}_{eff} oscillates with the same frequency as the axion field. Microwave cavities resonantly matched to the axion field can be built for $m_a \sim \mu\text{eV}$ [23], but for lower axion masses, the required cavity volume becomes impractically large. Resonant detection of lighter axions is possible in static-field setups if the resonant frequency and volume of the detector are independent, such as for lumped-element LC circuits [36–38]. However, their sensitivity to low-mass axions is suppressed by $\partial_t J_{\text{eff}} \propto m_a$.

Recently, we have proposed a new approach for axion DM detection, which uses frequency conversion to retain the advantages of resonant cavities while avoiding this suppression at low masses [39] (see also Refs. [40–42]).¹ A cavity is prepared by driving a “pump mode” with frequency $\omega_0 \sim \text{GHz}$, so that the axion can resonantly drive power into a “signal mode” of nearly degenerate frequency $\omega_1 \simeq \omega_0 \pm m_a$ and distinct spatial geometry. A scan over possible axion masses is performed by slightly perturbing

¹Resonant and broadband heterodyne setups based on optical interferometry have previously been proposed, but their sensitivity is limited by laser shot noise [43–45].

the cavity geometry, thereby modulating the frequency splitting $\omega_1 - \omega_0$. Compared to a static-field LC circuit of comparable volume and noise, the signal-to-noise ratio of this “heterodyne” approach is parametrically enhanced by ω_1/m_a . It also benefits from the very large intrinsic quality factors $Q_{\text{int}} \gtrsim 2 \times 10^{11}$ achievable in SRF cavities [46,47], which far exceed the quality factors achievable in static-field detectors targeting small axion masses.

In this work, we consider a broadband search where the signal and pump modes are fixed to be degenerate within their bandwidth, the feasibility of which is currently being investigated by the DarkSRF collaboration [48]. For the lowest axion masses, $m_a \lesssim \omega_0/Q_{\text{int}} \sim 10^{-17}$ eV, the signal power is resonantly enhanced. For higher axion masses, the signal is off resonance, but so are the dominant sources of noise in the cavity, thereby allowing this setup to explore new parameter space for axions as heavy as $m_a \sim 10^{-7}$ eV, as shown in Fig. 1. This broadband approach is thus

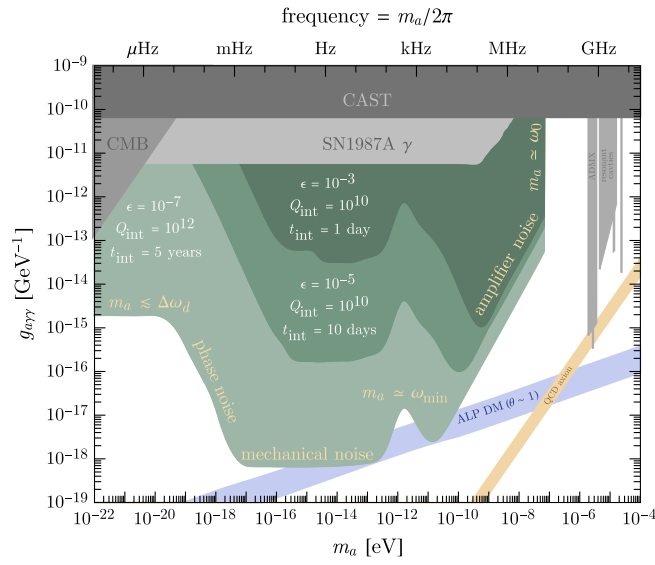


FIG. 1. In shaded green, the projected 90% C.L. reach of our setup to axion dark matter for several values of leakage noise suppression ϵ , intrinsic quality factor Q_{int} , and integration time t_{int} . For each set of parameters, we show the envelope of two or three distinct experimental runs, as discussed in the main text. We assume pump and signal mode frequencies $\omega_0 = \omega_1 = 100$ MHz, a cavity volume $V_{\text{cav}} = \text{m}^3$, a magnetic field strength $B_0 = 0.2$ T, a mode overlap form factor $\eta_a = 1$, shown in the Supplemental Material [49]. Existing constraints [18–27,50–54] are shown in gray. The orange band denotes parameter space motivated by the strong CP problem. Along the blue band, axions are produced through the misalignment mechanism at a level consistent with the observed dark matter density [55], assuming a temperature-independent mass, $\mathcal{O}(1)$ initial misalignment angle, and coupling $g_{a\gamma\gamma} = \alpha_{\text{em}}/(2\pi f_a)$. (For larger couplings, axions produced in the same way would make up a subcomponent of dark matter. However, since $J_{\text{eff}} \propto g_{a\gamma\gamma} \sqrt{\rho_a} \propto g_{a\gamma\gamma} f_a$, our setup is equally sensitive to such subcomponents.)

sensitive to a wide range of axion masses without the need to scan over frequency splittings. It is also the first approach that could directly detect electromagnetically coupled axion DM at the lowest viable DM masses $m_a \sim 10^{-22}$ eV, which correspond to a de Broglie wavelength the size of dwarf galaxies and a coherence time ten times longer than recorded human history. In this work, we will show parametric estimates that illustrate its potential; detailed calculations of signal and noise are given in Ref. [39] and the Supplemental Material [49].

II. DETECTION STRATEGY

The basic principle of our setup is shown in Fig. 2. The effective current, given by Eq. (2), oscillates at frequency $\omega_{\text{sig}} \simeq \omega_0 \pm m_a$. Since it is parallel to \mathbf{B}_0 , it drives power into the signal mode with strength parametrized by the form factor

$$\eta_a = \frac{|\int_{V_{\text{cav}}} \mathbf{E}_1^*(x) \cdot \mathbf{B}_0(x)|}{(\int_{V_{\text{cav}}} |\mathbf{E}_1(x)|^2 \int_{V_{\text{cav}}} |\mathbf{B}_0(x)|^2)^{1/2}} \leq 1, \quad (3)$$

where \mathbf{E}_1 is the signal mode electric field and V_{cav} is the volume of the cavity. We will be agnostic to the cavity geometry, taking $\omega_0 = \omega_1 \sim (1 \text{ m})^{-1} \sim 100$ MHz, but as a concrete example, $\eta_a \sim \mathcal{O}(1)$ for the TE_{011} and TM_{020} modes of a cylindrical cavity, which are degenerate in frequency for a length-to-radius ratio of $L/R \simeq 0.8$ [39,42].

We assume the frequencies of the pump and signal can be held fixed and degenerate within the signal mode bandwidth. However, the assumption of degeneracy only affects the reach at very low masses ($m_a \lesssim \omega_1/Q_1$). Furthermore, as shown in the Supplemental Material [49], even a frequency splitting 10^3 times larger than the bandwidth allows new ultralight axion parameter space to be

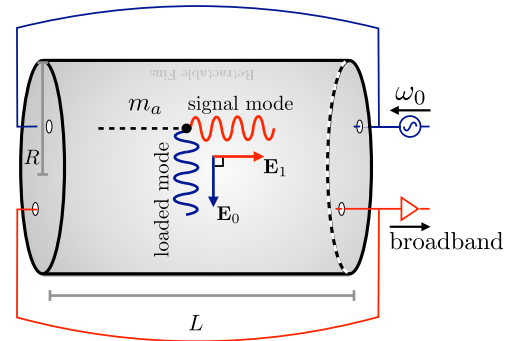


FIG. 2. A schematic depiction of our setup. A superconducting radio frequency (SRF) cavity is designed to have two degenerate modes of frequency ω_0 . It is prepared by driving a loading waveguide, predominantly coupled to the pump mode, with an external oscillator of frequency ω_0 . In the presence of axion DM, the pump mode magnetic field \mathbf{B}_0 sources an effective current that drives power into the signal mode. A wide range of axion masses can be simultaneously probed by broadband readout, via a readout waveguide predominantly coupled to the signal mode.

probed. The fundamental reason our setup can probe such low axion masses is that the signal strength depends on $\partial_r \mathbf{J}_{\text{eff}} \simeq g_{a\gamma\gamma} \partial_t a \partial_t^2 \mathbf{B} \propto m_a a \propto \sqrt{\rho_{\text{DM}}}$. For a fixed axion field amplitude, this vanishes as $m_a \rightarrow 0$, as required by general principles, but it is independent of m_a for fixed axion energy density.

When the sensitivities of a broadband and scanning approach overlap, the latter is stronger with a similar cavity [39], as expected on general grounds [56]. The two approaches have the same sensitivity only when m_a is smaller than the resonator bandwidth and the broadband setup functions as a resonant experiment. However, a broadband setup is simpler to operate due to its fixed geometry, and could be used as a stepping stone towards a scanning one. Moreover, it can probe a wide range of parameter space in a short integration time.

III. OVERVIEW OF SIGNAL AND NOISE

The frequency spread $\Delta\omega_{\text{sig}}$ of \mathbf{J}_{eff} (and hence of our signal) depends on the width $\Delta\omega_a$ of the axion field and the width $\Delta\omega_d$ of the oscillator driving the pump mode, $\Delta\omega_{\text{sig}} \sim \max(\Delta\omega_a, \Delta\omega_d)$. For concreteness, we take the power spectral density (PSD) of the central peak of the oscillator to be flat with a width $\Delta\omega_d \simeq 0.1$ mHz, comparable to a commercially available oscillator [57]. This is narrower than the signal mode width $\Delta\omega_r = \omega_0/Q_1$ for all parameters we consider. Since it can be beneficial to overcouple the readout, the loaded quality factor Q_1 of the signal mode can be much lower than the intrinsic quality factor Q_{int} , though the pump mode quality factor Q_0 remains comparable to Q_{int} .

The average signal power delivered to the cavity is

$$P_{\text{sig}} \sim \frac{(g_{a\gamma\gamma} n_a B_0)^2 \rho_{\text{DM}} V_{\text{cav}}}{\max(\Delta\omega_r, \Delta\omega_a)} \min \left[1, \left(\frac{\Delta\omega_r}{m_a} \right)^2 \right], \quad (4)$$

where B_0 is the characteristic amplitude of the pump mode magnetic field. The final factor in Eq. (4) accounts for the suppression that occurs when the axion drives the signal mode off resonance ($m_a \gtrsim \Delta\omega_r$). Given the signal power and noise PSD $S_n(\omega)$, the reach is determined by the signal-to-noise ratio (SNR) [58]:

$$\text{SNR} \sim \frac{P_{\text{sig}}}{S_n(\omega_{\text{sig}})} \sqrt{\frac{t_{\text{int}}}{\Delta\omega_{\text{sig}}}}, \quad (5)$$

where t_{int} is the total integration time. Equation (5) is valid when $t_{\text{int}} \gtrsim 1/\Delta\omega_{\text{sig}}$, which holds for all parameters we consider. A detailed derivation of the signal power and of the test statistic that Eq. (5) approximates is given in the Supplemental Material [49].

For most of the axion masses we consider, the dominant noise source is power in the oscillator or pump mode “leaking” into the readout waveguide. For instance, geometric imperfections can lead to small cross couplings $\epsilon \ll 1$

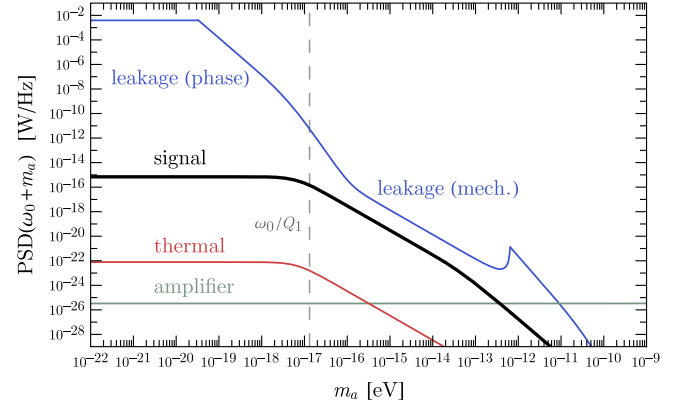


FIG. 3. The signal and noise PSDs evaluated at ω_{sig} as a function of the axion mass m_a , at critical coupling. The vertical dashed line denotes the bandwidth $\Delta\omega_r$ of the signal mode. We use a fixed, fiducial value of $g_{a\gamma\gamma}$, below our projected sensitivity, to allow the reader to easily compare the slopes of signal and noise. We show leakage noise (blue), thermal fluctuations of the electromagnetic field in the cavity at $T = 1.8$ K (red), and quantum-limited amplifier noise (green). Mechanical vibrations dominate the leakage noise for high m_a . The parameters are those of the second-lowest curve in Fig. 1.

between the loading architecture and signal mode (and similarly between the readout and pump mode), resulting in leakage noise power proportional to ϵ^2 . Leakage noise was previously encountered in the gravitational wave experiment MAGO, which looked for transitions between nearly degenerate symmetric and antisymmetric mode combinations of two identical SRF cavities coupled by a small tunable aperture [59–61]. The collaboration achieved a noise suppression of $\epsilon \sim 10^{-7}$ using magic tees and a variable phase shifter coupled to an active feedback loop [62]. In our setup, the two modes can additionally be chosen to be locally orthogonal, $\mathbf{E}_0 \cdot \mathbf{E}_1 = \mathbf{B}_0 \cdot \mathbf{B}_1 = 0$, with distinct spatial profiles, which could allow for further noise suppression by, e.g., loading/reading out the pump/signal mode near a node of the other mode [42], or by correlating readout measurements across multiple regions of the cavity. However, we conservatively consider $\epsilon \geq 10^{-7}$.

As shown in Fig. 3, leakage noise is largest when $m_a \lesssim \Delta\omega_d$, while for higher axion masses it falls off according to the tail of the pump mode PSD, which is determined by oscillator “phase noise” and mechanical vibrations of the cavity [39]. For the highest axion masses we consider, readout amplifier noise dominates. This explains the main qualitative features of Fig. 1. Since slightly different setups are optimal in each mass regime (with the exact crossover points depending on the experimental parameters), we organize the following discussion by axion mass.

IV. LOW-MASS AXIONS, $m_a \lesssim \Delta\omega_d$

When the axion mass is smaller than the oscillator width ($m_a \lesssim 10^{-19}$ eV), the signal overlaps in frequency with the

central peak of the oscillator. Both the signal and noise are spread over a bandwidth $\Delta\omega_{\text{sig}} \sim \Delta\omega_d$, giving a leakage noise PSD of

$$S_{\text{leak}}(\omega_{\text{sig}}) \sim \epsilon^2 P_{\text{in}} / \Delta\omega_d, \quad (6)$$

where $P_{\text{in}} \sim (\omega_0/Q_{\text{int}})B_0^2 V_{\text{cav}}$ is the power stored in the cavity. Assuming the readout waveguide is critically coupled to the signal mode ($Q_1 = Q_{\text{int}}/2$), which maximizes the sensitivity, Eq. (5) gives

$$\text{SNR} \sim \rho_{\text{DM}} \left(\frac{g_{a\gamma\gamma} Q_{\text{int}}}{\omega_0 \epsilon} \right)^2 \sqrt{t_{\text{int}} \Delta\omega_d} \quad (7)$$

and hence a reach $g_{a\gamma\gamma} \propto \epsilon/Q_{\text{int}}$, independent of m_a .²

Since leakage noise dominates, parameters such as B_0 , V_{cav} , and the cavity temperature do not directly affect the sensitivity. The same is true for external sources of low-frequency noise, such as vibrations of the ground or the cooling apparatus. Relative displacements of the cavity walls are suppressed by the rigidity of the cavity and further controlled by actively monitoring the mode frequencies and cross coupling ϵ . In the Supplemental Material [49], we conservatively estimate the effect of vibrational noise to be subdominant by many orders of magnitude in this mass range, in contrast to precision interferometric experiments where such noise can be dominant.

The signal and noise overlap in frequency, but can be distinguished by their distinct spatial profiles and spectral tails. There are several other effects to consider. Since $m_a \lesssim \Delta\omega_r$ in this regime, the axion field oscillates less than once per ring-up time of the cavity. Hence, the instantaneous signal power tracks the oscillations of $(\partial_t a)^2$, with angular frequency $2m_a$. Furthermore, $J_{\text{eff}} \propto B_0$ drives the signal mode on resonance, leading to a signal mode magnetic field $\pi/2$ out of phase with leakage noise. In addition, fluctuations in leakage noise due to fluctuations in the pump mode field can be monitored and ideally subtracted out. Thus, the parameter ϵ in Eq. (7) should be regarded as including the ability to distinguish between signal and leakage noise using these additional handles, though here we conservatively take $\epsilon \geq 10^{-7}$.

V. HIGH-MASS AXIONS, $m_a \gtrsim \text{kHz}$

Here, leakage and thermal noise are negligible due to the off-resonance suppression $(\Delta\omega_r/m_a)^2$. Since the axion is wider than the oscillator, the signal width is $\Delta\omega_{\text{sig}} \sim \Delta\omega_d$. As in static broadband axion searches in this mass range [32,37], amplifier noise dominates, such that

²The reach is slightly penalized when $\Delta\omega_d \lesssim 1/t_{\text{int}}$, as described in the Supplemental Material [49]. Furthermore, we do not consider very low axion masses $m_a \lesssim 1/t_{\text{int}}$, as the reach is strongly suppressed by the unknown instantaneous phase of the axion.

$$\text{SNR} \sim \rho_{\text{DM}} V_{\text{cav}} \frac{\Delta\omega_r}{S_{\text{amp}}(\omega_{\text{sig}})} \left(\frac{g_{a\gamma\gamma} B_0}{m_a} \right)^2 \sqrt{\frac{t_{\text{int}}}{\Delta\omega_d}}, \quad (8)$$

where for a quantum-limited amplifier, $S_{\text{amp}}(\omega) \sim \hbar\omega$. We cut off the reach in Fig. 1 at $m_a \simeq \omega_0$, above which higher harmonics of the cavity must be considered [40], as well as potential nonlinear response of the cavity walls [63].

The reach scales as $g_{a\gamma\gamma} \propto m_a^{5/4}/\Delta\omega_r^{1/2}$, assuming $\Delta\omega_r \gtrsim \Delta\omega_d$. Thus, when amplifier noise dominates, lowering Q_1 by overcoupling the signal mode to the readout is beneficial, as it reduces the off-resonance suppression of the signal without increasing the noise. The reach shown in Fig. 1 can be attained from a critically coupled run targeting low masses and an overcoupled run targeting high masses.³ For the latter run, we assume a quantum-limited amplifier, and take $Q_1 \sim 10^5$, which is a typical loaded quality factor of SRF cavities in accelerators [64].

VI. INTERMEDIATE-MASS AXIONS, $\Delta\omega_d \lesssim m_a \lesssim \text{kHz}$

For the bulk of the parameter space shown in Fig. 1, the reach is dictated by the high-frequency tail of the leakage noise. In most of this range, the oscillator is wider than the axion, so the signal width is $\Delta\omega_{\text{sig}} \sim \Delta\omega_d$.

In the lower end of this mass range, the main contribution to the leakage noise tail is from oscillator phase noise [39], which for $m_a \gtrsim \Delta\omega_r$ is of the form

$$S_{\text{leak}}(\omega_{\text{sig}}) \sim \epsilon^2 P_{\text{in}} \left(\frac{\Delta\omega_r}{m_a} \right)^2 S_{\varphi}(m_a), \quad (9)$$

where the phase noise PSD $S_{\varphi}(\omega)$ is parametrized by [65]

$$S_{\varphi}(\omega) = \sum_{n=0}^3 c_n \omega^{-n}, \quad (10)$$

and the c_n are fit to a commercially available oscillator [57]. For m_a slightly higher than $\Delta\omega_d$, the cubic term in $S_{\varphi}(\omega)$ dominates, resulting in $S_{\text{leak}}(\omega_{\text{sig}}) \propto 1/m_a^5$ and a rapid improvement in the reach at higher axion masses.

In the upper end of this mass range, the main noise contribution instead arises from displacements of the cavity walls, where mechanical vibrations at frequency m_a contribute to pump mode power at ω_{sig} [39]. On the basis of previous measurements in a MAGO prototype [59], we take the external mechanical force PSD to be spectrally flat, and the mechanical modes to have a quality factor $Q_m \sim 10^3$. As described in the Supplemental Material [49], the contribution of the lowest-lying mechanical resonance at $\omega_{\text{min}} \sim \text{kHz}$ dominates for $m_a \lesssim \omega_{\text{min}}$, such that

³The lowest curve in Fig. 1 requires a third run with intermediate overcoupling, specifically targeting intermediate mass axions.

$$S_{\text{leak}}(\omega_{\text{sig}}) \sim \epsilon^2 P_{\text{in}} \left(\frac{\Delta\omega_r}{m_a} \right)^2 \frac{\delta^2 Q_{\text{int}}^2}{\omega_{\text{min}} Q_m}, \quad (11)$$

where $\delta \ll 1$ is the fractional displacement of the cavity walls. For $\Delta\omega_a \lesssim \Delta\omega_r \lesssim m_a$, $P_{\text{sig}} \propto 1/m_a^2$, and thus the sensitivity in this region is independent of the axion mass. For frequencies above ω_{min} , we assume a forest of evenly spaced mechanical modes exists. To estimate δ , we note that the DarkSRF collaboration has recently demonstrated the ability to control the resonant frequency of a driven cavity to one part in $Q_{\text{int}} \gtrsim 10^{10}$, corresponding to sub-nanometer displacements of the cavity walls [48,66]. This has been demonstrated on minute timescales, and a near-future run is expected to prolong this to $\mathcal{O}(1)$ week. Thus, we fix the typical rms cavity wall displacement to $q_{\text{rms}} = 0.1$ nm, corresponding to $\delta \sim 10^{-10}$ for a meter-sized cavity. This is larger than the displacement due to environmental seismic noise [67], reflecting the expectation that vibrations will primarily arise from the apparatus itself (e.g., the helium pump).

Deformations of the cavity walls can also directly transfer power between the pump and signal modes. This “mode mixing” is parametrized by a dimensionless mechanical form factor η_{mix} , with $S_{\text{mix}} \sim (\eta_{\text{mix}}/\epsilon)^2 S_{\text{leak}}$. The form factor η_{mix} vanishes for a perfectly cylindrical cavity, which implies its value is set by cavity deformations [60,68]. Since ϵ parametrizes the precision to which we can control slow deformations of the cavity and waveguide geometry, we expect $\eta_{\text{mix}} \sim \epsilon$, such that mode mixing is at most comparable to mechanical leakage noise.

VII. DISCUSSION

We have proposed a heterodyne approach to search for ultralight axion dark matter through its coupling to electromagnetism, which applies recent developments in the manufacturing and control of SRF cavities. Due to the decreasing signal power and increasing strength of readout noise at low frequencies, traditional static-field haloscopes

have limited reach to axions lighter than a kHz $\sim 10^{-12}$ eV [31,32]. In contrast, our setup is sensitive to much lighter axions, including the entire allowed mass range for fuzzy dark matter, $m_a \geq \mathcal{O}(10^{-21})$ eV [69–74], thereby complementing ultralight axion searches that use nonelectromagnetic couplings [75–78]. It is also sensitive to axions as heavy as 10^{-7} eV, including those motivated by string theory [79] and the misalignment mechanism. Finally, the broadband nature of this approach implies that a network of such detectors would be sensitive to axion-induced transients, due to miniclusters or topological defects [80,81].

Our projections rely on noise estimates anchored to experimental findings, such as those obtained 15 yr ago by the MAGO Collaboration [59–61]. More recently, there has been renewed interest in the SRF community to apply their technological advances to new physics searches, leading to the recent results of the DarkSRF collaboration [48] that show the feasibility of our proposed approach. The promising sensitivity of SRF cavities to weakly coupled physics, demonstrated in this work, motivates *in situ* measurements of mode mixing and leakage noise, in order to further investigate the potential of these ideas. Future developments, some of which are already envisioned by the DarkSRF collaboration, can further extend our reach, improving the capacity to probe some of the most motivated dark matter candidates.

ACKNOWLEDGMENTS

We thank Saptarshi Chaudhuri, Peter Graham, Roni Harnik, Robert Lasenby, Christopher Nantista, Jeffrey Neilson, Philip Schuster, Sami Tantawi, and Natalia Toro for valuable discussions. A. B. is supported by the James Arthur Fellowship. S. A. R. E. is supported by the U.S. Department of Energy under Contract No. DE-AC02-76SF00515 and by the Swiss National Science Foundation, SNF Project No. P400P2_186678. K. Z. is supported by the NSF GRFP under Grant No. DGE-1656518.

-
- [1] F. Zwicky, Die Rotverschiebung von extragalaktischen Nebeln, *Helv. Phys. Acta* **6**, 110 (1933).
 - [2] P. Svrcek and E. Witten, Axions in string theory, *J. High Energy Phys.* **06** (2006) 051.
 - [3] A. Arvanitaki, S. Dimopoulos, S. Dubovsky, N. Kaloper, and J. March-Russell, String Axiverse, *Phys. Rev. D* **81**, 123530 (2010).
 - [4] M. J. Stott, D. J. E. Marsh, C. Pongkitivanichkul, L. C. Price, and B. S. Acharya, Spectrum of the axion dark sector, *Phys. Rev. D* **96**, 083510 (2017).
 - [5] R. D. Peccei and H. R. Quinn, *CP* Conservation in the Presence of Instantons, *Phys. Rev. Lett.* **38**, 1440 (1977).
 - [6] R. D. Peccei and H. R. Quinn, Constraints imposed by *CP* conservation in the presence of instantons, *Phys. Rev. D* **16**, 1791 (1977).
 - [7] S. Weinberg, A New Light Boson? *Phys. Rev. Lett.* **40**, 223 (1978).
 - [8] F. Wilczek, Problem of Strong *P* and *T* Invariance in the Presence of Instantons, *Phys. Rev. Lett.* **40**, 279 (1978).

- [9] J. Preskill, M. B. Wise, and F. Wilczek, Cosmology of the invisible axion, *Phys. Lett.* **120B**, 127 (1983).
- [10] L. F. Abbott and P. Sikivie, A cosmological bound on the invisible axion, *Phys. Lett.* **120B**, 133 (1983).
- [11] M. Dine and W. Fischler, The not so harmless axion, *Phys. Lett.* **120B**, 137 (1983).
- [12] P. W. Graham, D. E. Kaplan, and S. Rajendran, Cosmological Relaxation of the Electroweak Scale, *Phys. Rev. Lett.* **115**, 221801 (2015).
- [13] N. Fonseca and E. Morgante, Relaxion dark matter, *Phys. Rev. D* **100**, 055010 (2019).
- [14] A. Banerjee, H. Kim, and G. Perez, Coherent relaxion dark matter, *Phys. Rev. D* **100**, 115026 (2019).
- [15] J. Goodman, Repulsive dark matter, *New Astron.* **5**, 103 (2000).
- [16] W. Hu, R. Barkana, and A. Gruzinov, Cold and Fuzzy Dark Matter, *Phys. Rev. Lett.* **85**, 1158 (2000).
- [17] L. Hui, J. P. Ostriker, S. Tremaine, and E. Witten, Ultralight scalars as cosmological dark matter, *Phys. Rev. D* **95**, 043541 (2017).
- [18] V. Anastassopoulos *et al.* (CAST Collaboration), New CAST limit on the axion-photon interaction, *Nat. Phys.* **13**, 584 (2017).
- [19] C. Hagmann *et al.* (ADMX Collaboration), Results from a High Sensitivity Search for Cosmic Axions, *Phys. Rev. Lett.* **80**, 2043 (1998).
- [20] C. Boutan *et al.* (ADMX Collaboration), Piezoelectrically Tuned Multimode Cavity Search for Axion Dark Matter, *Phys. Rev. Lett.* **121**, 261302 (2018).
- [21] N. Du *et al.* (ADMX Collaboration), A Search for Invisible Axion Dark Matter with the Axion Dark Matter Experiment, *Phys. Rev. Lett.* **120**, 151301 (2018).
- [22] B. M. Brubaker *et al.*, First Results from a Microwave Cavity Axion Search at 24 μeV , *Phys. Rev. Lett.* **118**, 061302 (2017).
- [23] T. Braine *et al.* (ADMX Collaboration), Extended Search for the Invisible Axion with the Axion Dark Matter Experiment, *Phys. Rev. Lett.* **124**, 101303 (2020).
- [24] S. DePanfilis, A. C. Melissinos, B. E. Moskowitz, J. T. Rogers, Y. K. Semertzidis, W. U. Wuensch, H. J. Halama, A. G. Prodell, W. B. Fowler, and F. A. Nezrick, Limits on the Abundance and Coupling of Cosmic Axions at $m_a \mu\text{eV}$, *Phys. Rev. Lett.* **59**, 839 (1987).
- [25] W. Wuensch, S. De Panfilis-Wuensch, Y. K. Semertzidis, J. T. Rogers, A. C. Melissinos, H. J. Halama, B. E. Moskowitz, A. G. Prodell, W. B. Fowler, and F. A. Nezrick, Results of a laboratory search for cosmic axions and other weakly coupled light particles, *Phys. Rev. D* **40**, 3153 (1989).
- [26] C. Hagmann, P. Sikivie, N. S. Sullivan, and D. B. Tanner, Results from a search for cosmic axions, *Phys. Rev. D* **42**, 1297 (1990).
- [27] L. Zhong *et al.* (HAYSTAC Collaboration), Results from phase 1 of the HAYSTAC microwave cavity axion experiment, *Phys. Rev. D* **97**, 092001 (2018).
- [28] B. D. Blout, E. J. Daw, M. P. Decowski, P. T. P. Ho, L. J. Rosenberg, and D. B. Yu, A radio telescope search for axions, *Astrophys. J.* **546**, 825 (2001).
- [29] A. Abramowski *et al.* (H.E.S.S. Collaboration), Constraints on axionlike particles with H.S.S.S. from the irregularity of the pks 2155 – 304 energy spectrum, *Phys. Rev. D* **88**, 102003 (2013).
- [30] M. Ajello *et al.* (The Fermi-LAT Collaboration), Search for Spectral Irregularities due to Photon–Axionlike-Particle Oscillations with the Fermi Large Area Telescope, *Phys. Rev. Lett.* **116**, 161101 (2016).
- [31] J. L. Ouellet *et al.*, First Results from ABRACADABRA-10 cm: A Search for Sub- μeV Axion Dark Matter, *Phys. Rev. Lett.* **122**, 121802 (2019).
- [32] A. V. Gramolin, D. Aybas, D. Johnson, J. Adam, and A. O. Sushkov, Search for axion-like dark matter with ferromagnets, *Nat. Phys.* **17**, 79 (2021).
- [33] C. A. Thomson, B. T. McAllister, M. Goryachev, E. N. Ivanov, and M. E. Tobar, Upconversion Loop Oscillator Axion Detection Experiment: A Precision Frequency Interferometric Axion Dark Matter Search with a Cylindrical Microwave Cavity, *Phys. Rev. Lett.* **126**, 081803 (2021); Erratum, *Phys. Rev. Lett.* **127**, 019901 (2021).
- [34] P. Sikivie, Experimental Tests of the Invisible Axion, *Phys. Rev. Lett.* **51**, 1415 (1983).
- [35] P. Sikivie, Detection Rates for “Invisible” Axion Searches, *Phys. Rev. D* **32**, 2988 (1985); Erratum, *Phys. Rev. D* **36**, 974 (1987).
- [36] P. Sikivie, N. Sullivan, and D. B. Tanner, Proposal for Axion Dark Matter Detection Using an LC Circuit, *Phys. Rev. Lett.* **112**, 131301 (2014).
- [37] Y. Kahn, B. R. Safdi, and J. Thaler, Broadband and Resonant Approaches to Axion Dark Matter Detection, *Phys. Rev. Lett.* **117**, 141801 (2016).
- [38] S. Chaudhuri, K. D. Irwin, P. W. Graham, and J. Mardon, Optimal electromagnetic searches for axion and hidden-photon dark matter, [arXiv:1904.05806](https://arxiv.org/abs/1904.05806).
- [39] A. Berlin, R. T. D’Agnolo, S. A. R. Ellis, C. Nantista, J. Neilson, P. Schuster, S. Tantawi, N. Toro, and K. Zhou, Axion dark matter detection by superconducting resonant frequency conversion, *J. High Energy Phys.* **07** (2020) 088.
- [40] P. Sikivie, Superconducting radio frequency cavities as axion dark matter detectors, [arXiv:1009.0762](https://arxiv.org/abs/1009.0762).
- [41] Z. Bogorad, A. Hook, Y. Kahn, and Y. Soreq, Probing Axionlike Particles and the Axiverse with Superconducting Radio-Frequency Cavities, *Phys. Rev. Lett.* **123**, 021801 (2019).
- [42] R. Lasenby, Microwave cavity searches for low-frequency axion dark matter, *Phys. Rev. D* **102**, 015008 (2020).
- [43] W. DeRocco and A. Hook, Axion interferometry, *Phys. Rev. D* **98**, 035021 (2018).
- [44] I. Obata, T. Fujita, and Y. Michimura, Optical Ring Cavity Search for Axion Dark Matter, *Phys. Rev. Lett.* **121**, 161301 (2018).
- [45] H. Liu, B. D. Elwood, M. Evans, and J. Thaler, Searching for axion dark matter with birefringent cavities, *Phys. Rev. D* **100**, 023548 (2019).
- [46] A. Romanenko, A. Grassellino, A. C. Crawford, D. A. Sergatskov, and O. Melnychuk, Ultra-high quality factors in superconducting niobium cavities in ambient magnetic fields up to 190 mG, *Appl. Phys. Lett.* **105**, 234103 (2014).
- [47] S. Posen, G. Wu, E. Harms, A. Grassellino, O. S. Melnychuk, D. A. Sergatskov, N. Solyak, A. Palczewski, D. Gonnella, and T. Peterson, Role of magnetic flux expulsion to reach

- $Q_0 > 3 \times 10^{10}$ in superconducting rf cryomodules, *Phys. Rev. Accel. Beams* **22**, 032001 (2019).
- [48] A. Grassellino, SRF-based dark matter search: Experiment, 2020, <https://indico.physics.lbl.gov/event/939/contributions/4371/attachments/2162/2915/DarkSRF-Aspen-2.pdf>.
- [49] See Supplemental Material at <http://link.aps.org/supplemental/10.1103/PhysRevD.104.L111701> for detailed pedagogical derivations of important results discussed throughout the paper.
- [50] S. J. Asztalos, R. F. Bradley, L. Duffy, C. Hagmann, D. Kinion, D. M. Moltz, L. J. Rosenberg, P. Sikivie, W. Stoeffl, N. S. Sullivan, D. B. Tanner, K. van Bibber, and D. B. Yu, Improved rf cavity search for halo axions, *Phys. Rev. D* **69**, 011101 (2004).
- [51] B. T. McAllister, G. Flower, E. N. Ivanov, M. Goryachev, J. Bourhill, and M. E. Tobar, The ORGAN experiment: An axion haloscope above 15 GHz, *Phys. Dark Universe* **18**, 67 (2017).
- [52] M. A. Fedderke, P. W. Graham, and S. Rajendran, Axion dark matter detection with CMB polarization, *Phys. Rev. D* **100**, 015040 (2019).
- [53] G. G. Raffelt, Stars as Laboratories for Fundamental Physics (1996), <http://wwwth.mpp.mpg.de/members/raffelt/mypapers/199613.pdf>.
- [54] A. Payez, C. Evoli, T. Fischer, M. Giannotti, A. Mirizzi, and A. Ringwald, Revisiting the SN1987A gamma-ray limit on ultralight axion-like particles, *J. Cosmol. Astropart. Phys.* **02** (2015) 006.
- [55] N. Blinov, M. J. Dolan, P. Draper, and J. Kozaczuk, Dark matter targets for axionlike particle searches, *Phys. Rev. D* **100**, 015049 (2019).
- [56] S. Chaudhuri, K. Irwin, P. W. Graham, and J. Mardon, Fundamental limits of electromagnetic axion and hidden-photon dark matter searches: Part I—The quantum limit, [arXiv:1803.01627](https://arxiv.org/abs/1803.01627).
- [57] Berkeley Nucleonics Corporation, Model 865-M Wideband Synthesizer Data Sheet, 2019, https://www.berkeleyelectronics.com/sites/default/files/products/datasheets/865-m_datasheet_5-3-19_v1.04.pdf.
- [58] R. H. Dicke, The measurement of thermal radiation at microwave frequencies, *Rev. Sci. Instrum.* **17**, 268 (1946).
- [59] P. Bernard, G. Gemme, R. Parodi, and E. Picasso, A Detector of small harmonic displacements based on two coupled microwave cavities, *Rev. Sci. Instrum.* **72**, 2428 (2001).
- [60] P. Bernard, A. Chincarini, G. Gemme, R. Parodi, and E. Picasso, A detector of gravitational waves based on coupled microwave cavities, [arXiv:gr-qc/0203024](https://arxiv.org/abs/2003024).
- [61] R. Ballantini *et al.*, Microwave apparatus for gravitational waves observation, [arXiv:gr-qc/0502054](https://arxiv.org/abs/gr-qc/0502054).
- [62] P. Bernard, G. Gemme, R. Parodi, and E. Picasso, The RF control and detection system for PACO the parametric converter detector, [arXiv:physics/0004031](https://arxiv.org/abs/physics/0004031).
- [63] D. Eriksson, G. Brodin, M. Marklund, and L. Stenflo, A possibility to measure elastic photon-photon scattering in vacuum, *Phys. Rev. A* **70**, 013808 (2004).
- [64] H. Padamsee, *RF Superconductivity: Science, Technology, and Applications* (John Wiley & Sons, New York, 2009).
- [65] E. Rubiola, *Phase Noise and Frequency Stability in Oscillators* (Cambridge University Press, Cambridge, England, 2009).
- [66] A. Grassellino, SRF-based dark matter search: Experiment, 2019, <https://indico.fnal.gov/event/19433/session/2/contribution/2/material/slides/0.pdf>.
- [67] P. R. Saulson, *Fundamentals of Interferometric Gravitational Wave Detectors*, 2nd ed., (World Scientific, Singapore, 2017).
- [68] D. Meidlinger, A General Perturbation Theory for Cavity Mode Field Patterns, 2009, <https://accelconf.web.cern.ch/SRF2009/papers/thppo005.pdf>.
- [69] E. Armengaud, N. Palanque-Delabrouille, C. Yèche, D. J. Marsh, and J. Baur, Constraining the mass of light bosonic dark matter using SDSS Lyman- α forest, *Mon. Not. R. Astron. Soc.* **471**, 4606 (2017).
- [70] V. Iršič, M. Viel, M. G. Haehnelt, J. S. Bolton, and G. D. Becker, First Constraints on Fuzzy Dark Matter from Lyman- α Forest Data and Hydrodynamical Simulations, *Phys. Rev. Lett.* **119**, 031302 (2017).
- [71] M. Nori, R. Murgia, V. Iršič, M. Baldi, and M. Viel, Lyman α forest and non-linear structure characterization in fuzzy dark matter cosmologies, *Mon. Not. R. Astron. Soc.* **482**, 3227 (2019).
- [72] A. Garzilli, O. Ruchayskiy, A. Magalich, and A. Boyarsky, How warm is too warm? Towards robust Lyman- α forest bounds on warm dark matter, [arXiv:1912.09397](https://arxiv.org/abs/1912.09397).
- [73] D. J. Marsh and J. C. Niemeyer, Strong Constraints on Fuzzy Dark Matter from Ultrafaint Dwarf Galaxy Eridanus II, *Phys. Rev. Lett.* **123**, 051103 (2019).
- [74] K. Schutz, Subhalo mass function and ultralight bosonic dark matter, *Phys. Rev. D* **101**, 123026 (2020).
- [75] P. W. Graham, D. E. Kaplan, J. Mardon, S. Rajendran, W. A. Terrano, L. Trahms, and T. Wilkason, Spin precession experiments for light axionic dark matter, *Phys. Rev. D* **97**, 055006 (2018).
- [76] T. Wu *et al.*, Search for Axionlike Dark Matter with a Liquid-State Nuclear Spin Comagnetometer, *Phys. Rev. Lett.* **122**, 191302 (2019).
- [77] W. A. Terrano, E. G. Adelberger, C. A. Hagedorn, and B. R. Heckel, Constraints on Axionlike Dark Matter with Masses Down to 10- 23 ev/c^2 , *Phys. Rev. Lett.* **122**, 231301 (2019).
- [78] C. Abel *et al.*, Search for Axionlike Dark Matter through Nuclear Spin Precession in Electric and Magnetic Fields, *Phys. Rev. X* **7**, 041034 (2017).
- [79] J. Halverson, C. Long, B. Nelson, and G. Salinas, Towards string theory expectations for photon couplings to axionlike particles, *Phys. Rev. D* **100**, 106010 (2019).
- [80] M. Pospelov, S. Pustelny, M. P. Ledbetter, D. F. Jackson Kimball, W. Gawlik, and D. Budker, Detecting Domain Walls of Axionlike Models Using Terrestrial Experiments, *Phys. Rev. Lett.* **110**, 021803 (2013).
- [81] D. F. Jackson Kimball, D. Budker, J. Eby, M. Pospelov, S. Pustelny, T. Scholtes, Y. V. Stadnik, A. Weis, and A. Wickenbrock, Searching for axion stars and Q-balls with a terrestrial magnetometer network, *Phys. Rev. D* **97**, 043002 (2018).